ADVANCED ENERGY MATERIALS
www.advenergymat.de

Influence of Grain Size on Phase Transitions in Halide Perovskite Films

*Camille Stavrakas, Szymon J. Zelewski, Kyle Frohna, Edward P. Booker, Krzysztof Galkowski, Kangyu Ji, Edoardo Ruggeri, Sebastian Mackowski, Robert Kudrawiec, Paulina Plochocka, and Samuel D. Stranks**

Grain size in polycrystalline halide perovskite films is known to have an impact on the optoelectronic properties of the films, but its influence on their soft structural properties and phase transitions is unclear. Here, temperature-dependent X-ray diffraction, absorption, and macro- and micro-photoluminescence measurements are used to investigate the tetragonal to orthorhombic phase transition in thin methylammonium lead iodide films with grain sizes ranging from the micrometer scale down to the tens of nanometer scale. It is shown that the phase transition nominally at ≈150 K is increasingly suppressed with decreasing grain size and, in the smallest grains, the first evidence of a phase transition is only seen at temperatures as low as ≈80 K. With decreasing grain size, an increasing magnitude of the hysteresis is also seen in the structural and optoelectronic properties when cooling to, and then upon heating from, 100 K. This work reveals the remarkable sensitivity of the optoelectronic, physical, and phase properties to the local environment of the perovskite structure, which will have large ramifications for phase and defect engineering in operating devices.

In the quest for a cheaper though versatile and high-performance alternative to silicon-based optoelectronics, metal halide perovskites hold promise. Extensive research efforts directed toward the optimization of perovskite thin film growth from simple precursors have improved the efficiency and stability of devices to a high quality standard and low cost, placing them on the verge of commercialization.[1–6] Nevertheless, a better understanding of what influences their crystalline structure is needed in order to achieve phase purity, manage defects, and ultimately achieve optimal device performances.

The dramatic gain in solar cell device efficiency since 2012 is only one of the features making perovskites stand out among other photovoltaic materials. With a Young's modulus around 20 GPa,[7–10] perovskites are mechanically softer than most other PV materials such as silicon (>160 GPa),[11,12] GaAs (≈85 GPa),[13] CIGS (≈80 GPa),[14,15] and CdTe (≈40 GPa),[16,17] and their structure has been reported to be prone to light-induced, electric-field-induced, and temperature-dependent rearrangements.[18–23] The workhorse system studied to date, methylammonium lead iodide ($MAPbI_3$), is in a tetragonal phase (TP) at room temperature, but undergoes a transition to a cubic phase at high temperature (≈330 K) and an orthorhombic phase (OP) at low temperature (≈150 K). Recently, we and others[24–26] have reported that the structural rearrangement from TP to OP causes a distinct hysteretic change in optical and transport properties as well as device behavior between heating and cooling cycles. This hysteresis could be reduced by scraping the film from the substrate and instead measuring randomly oriented powder samples.[24] These results provide hints that the thermal stability[27] and phase transition can be influenced by the local environment of the film due to interactions between the material and substrate as well as within the bulk film itself. Unless understood and mitigated, such hysteretic changes at low temperature may limit the use of perovskite solar cells in some specific applications, for example, aerospace applications, which require operation at extremely low temperatures[28] (<200 K).

State-of-the-art perovskite films are polycrystalline, which leads to microscale inhomogeneities in a number of properties such as morphology and defect distributions[29–32] and, in turn, to local variations in the electronic environment for charge carriers. Generally, increasing grain sizes in $MAPbI_3$ films has resulted in improvements in critical performance parameters, such as an increase in carrier mobility and charge collection efficiency,[33,34] along with smaller bandgaps, longer lifetimes,

C. Stavrakas, K. Frohna, Dr. E. P. Booker, Dr. K. Galkowski, K. Ji, E. Ruggeri, Dr. S. D. Stranks
Cavendish Laboratory
JJ Thomson Avenue, Cambridge CB3 0HE, UK
E-mail: sds65@cam.ac.uk
S. J. Zelewski, Prof. R. Kudrawiec
Faculty of Fundamental Problems of Technology
Wroclaw University of Science and Technology
Wybrzeże Wyspiańskiego 27, 50-370 Wrocław, Poland
S. J. Zelewski, Dr. P. Plochocka
Laboratoire National des Champs Magnetiques Intenses
CNRS-UJF-UPS-INSA
143 avenue de Rangueil, 31400 Toulouse, France
Dr. K. Galkowski, Prof. S. Mackowski
Institute of Physics
Faculty of Physics
Astronomy and Informatics
Nicolaus Copernicus University
5th Grudziadzka St.,87-100 Torun, Poland
The ORCID identification number(s) for the author(s) of this article can be found under https://doi.org/10.1002/aenm.201901883.

DOI: 10.1002/aenm.201901883

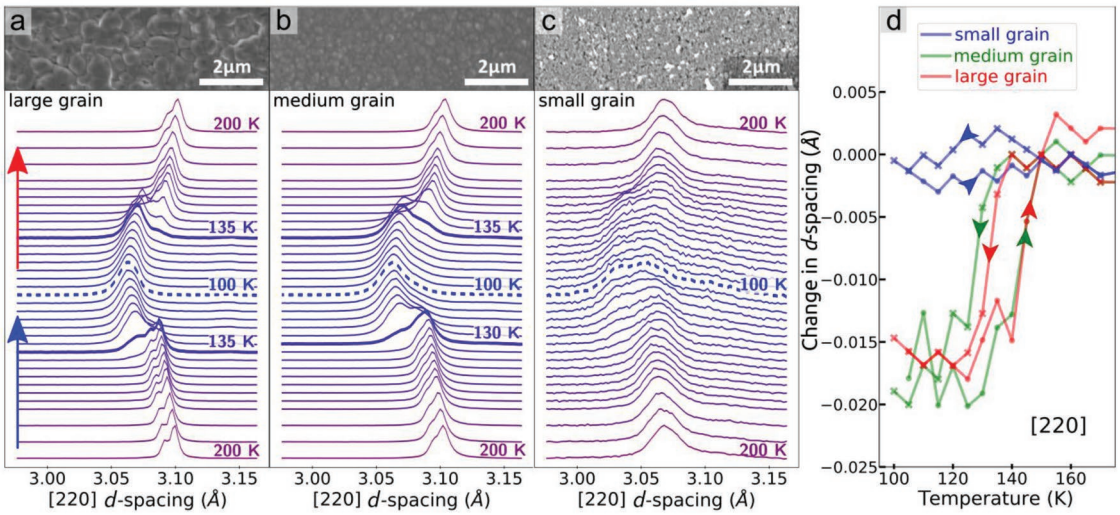

Figure 1. Temperature-dependent X-ray diffractograms (normalized to their respective maximum) around the [220] reflection of $MAPbI_3$ thin films of varying grain size: a) less than 50 nm, b) ≈100 nm, and c) 0.5–1 μm, where the lattice spacing was calculated from the measured 2θ angle. The blue and red arrows (panel a) indicate the temperature cycle from room temperature to 100 K and back to room temperature, respectively. The distance between each diffractogram is proportional to the temperature step, and the phase transition onsets are highlighted in bold. The insets in (a), (b), and (c) show SEM images of the films. d) A comparison of the hysteretic change in *d*-spacing with respect to the linear shift above the transition temperature (Figure S1, Supporting Information) for each film, with weighted averages used to extract the value in the presence of mixed peaks (i.e., when both OP and TP peaks are present).

and higher absorption coefficients.[35] Nevertheless, an understanding of the underpinning differences in structural and mechanical properties of bulk films with different grain sizes, and how grain size influences their crystal phase heterogeneity, is still lacking. Furthermore, varying the grain size without otherwise changing the material composition provides a controllable lever to vary the local environment and thus systematically investigate the link between the local surroundings and the hysteretic phase transition phenomena.

In this letter, we investigate the influence of the grain size on the nature of the TP to OP phase transition in $MAPbI_3$ perovskite polycrystalline thin films, with grains sizes ranging across two orders of magnitude from tens of nanometers to micrometer scale. We characterize the changes in structural and optoelectronic properties of these films by means of temperature-dependent X-ray diffraction (XRD), optical absorption, as well as macro- and micro-photoluminescence (PL) measurements. Our results reveal that the phase transition is increasingly suppressed with decreasing grain size. We also find that the temperature range of the hysteresis of the phase transition between the heating and cooling cycles increases with decreasing grain size. These results provide strong evidence that the phase transition and optoelectronic properties are significantly influenced by the local grain environment of the material, and reveal new insights to control the phase and optoelectronic behavior in these mechanically "soft" semiconductors.

We solution-processed thin films of $MAPbI_3$ of varying grain size on glass substrates by modifying recipes involving lead acetate and methylammonium iodide precursors (see Methods and Table S1 in the Supporting Information for full details). Samples with a grain size on the order of tens of nanometers (small grain) were obtained by confining the perovskite, deposited with a lead acetate recipe, within a mesoporous scaffold of Al_2O_3 nanoparticles (≈50 nm in size). Medium grain (≈100 nm) films were fabricated as planar films with the same lead acetate recipe, and large grain films (≈0.5–1 μm) were made in the same way but by adding hypophosphorous acid to the lead-acetate-based precursor solution following previous methods to achieve enhanced grain growth without otherwise changing the electronic structure or optical bandgap properties.[36] Scanning electron microscope (SEM) images of these films are shown as insets in **Figure 1**a (large grain), 1b (medium grain), and 1c (small grain). We note that grain size is defined here as morphological grain size ascertained from SEM images; identifying true grain size would require local diffraction approaches.[37] We herein present temperature-dependent XRD and optical absorption measurements on each sample following the same temperature cycle rate as well as macro- and micro-PL measurements from 300 down to 100 K and back up to 300 K (see Table S2 of the Supporting Information for more details).

In Figure 1, we show structural changes from temperature-dependent XRD measurements (normalized to their respective maximum) on large grain (Figure 1a), medium grain (Figure 1b), and small grain (Figure 1c) films over the temperature range of 100–200 K (see Figure S1 of the Supporting Information for the full temperature range of 100–300 K). The stated lattice spacing (*d*-spacing) was calculated from the measured 2θ diffraction angle of the [220] reflection; we note that we also observe the same trends for the [110] reflection (Figure S3, Supporting Information). The distance between each diffractogram is proportional to the temperature step and blue and red arrows indicate the cooling and heating cycles, respectively. The phase transition onsets are highlighted in bold in Figure 1a,b. We find that the first onset of a phase transition to the orthorhombic phase during the cooling cycle is at the highest temperature for the large grain

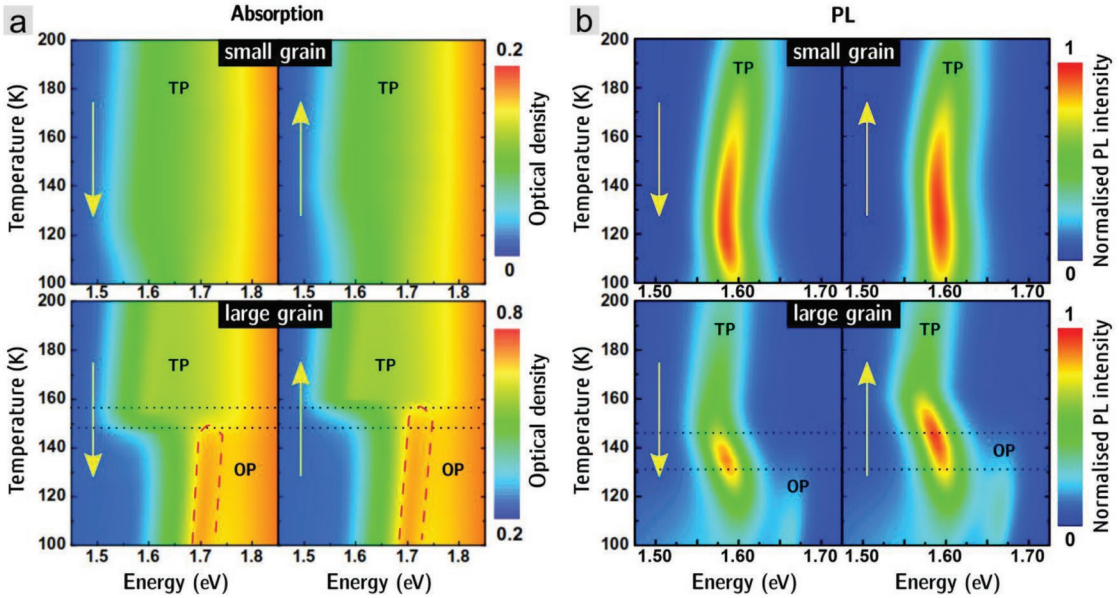

Figure 2. a) Temperature-dependent optical absorption and b) macro-PL measurements on small grain (top panels) and large grain (bottom panels) $MAPbI_3$ thin films. Yellow arrows indicate the temperature cycle from 300 down to 100 K and back up to 300 K with a rate of 2 K min^{-1} and a dwell time of 5 min. Absorption spectra are displayed with a color scale representing the measured optical density. PL maps for each sample are normalized to the maximum PL intensity measured during the temperature cycle. For all macro-PL measurements, the films were excited with a 532 nm diode laser with an excitation density of 0.6 mW cm^{-2}. Black dotted lines show the phase transition onsets and red dashed lines highlight the excitonic emission.

sample (135 K), followed by the medium grain film at the slightly lower temperature of 130 K. Upon heating, both samples start the transition back to the tetragonal phase at a similar temperature (135 K). Surprisingly, although we observe a shift in *d*-spacing of the TP peak with temperature from ≈145 K (cooling) to 100 K and back to 145 K (heating), the *d*-spacing change between the end points of the hysteresis for the small grain sample is consistent with a suppression of the phase transition.

We track the position of the [220] reflection and compare the hysteretic change in *d*-spacing for each sample in Figure 1d. Around the phase transition, where both TP and OP peaks are present, we follow the average *d*-spacing weighted by the amplitudes of both contributions (see Methods and Figure S1 of the Supporting Information). This comparison suggests that the phase transition is increasingly suppressed and the width of the hysteresis between cooling and heating cycles increases as the grain size decreases. Indeed, we observe a hysteresis in structural properties between the two temperature cycles across a temperature range of ≈25 K for the large grain, ≈30 K for the medium grain, and ≈45 K for the small grain samples. We propose that the suppression of the phase transition and widened hysteresis in the small grain samples is due to the grains being mechanically constrained in the mesopores and therefore cannot structurally rearrange as easily as in the other samples.

We also note that we observe a mixed phase of both TP and OP across a temperature span of 10 K during the cooling (from 130 to 120 K) and heating (from 135 to 145 K) cycles in the medium grain film, while in the large grain sample we observe this mixing across 10 K during the cooling cycle (from 135 to 125 K) and 15 K during the heating cycle (from 135 to 150 K), as displayed in Figure S4 of the Supporting Information. This asymmetry in the large grain sample is followed by a positive shift in *d*-spacing remaining until room temperature, indicating that the large grain structure does not transform back to its initial lattice parameters. This structural rearrangement appears however to be transient as the original *d*-spacing is recovered after relaxation at room temperature (see Figure S4, Supporting Information).

In order to investigate how the structural phase transition and hysteresis observations manifest themselves on optoelectronic properties, we performed temperature-dependent absorption and PL measurements. We compare the temperature-dependent absorption (**Figure 2**a) and PL (Figure 2b) of the two extreme cases: the small grain (top panels) and the large grain (bottom panels) films (see Figures S4–S6 of the Supporting Information for a comparison of all three grain sizes). These 2D colormaps represent the spectra as measured in both absorption and PL, with a signal intensity ranging linearly from blue (low) to red (high). Yellow arrows indicate the temperature cycle from room temperature (300 K) to 100 K and back up to room temperature. The temperature steps as well as the cycle rate were the same as the parameters used for XRD measurements (see Table S2, Supporting Information). In the case of the small grain film, consistent with XRD measurements, we do not observe any clear indication of a phase transition in this temperature range despite a small shift in both absorption onset and PL energy (top panels in Figure 2a,b, respectively). Further measurements carried out at lower temperatures show slight PL peak broadening that may be the signature of the formation of the orthorhombic phase below 80 K (see Figure S8, Supporting Information). By contrast, the results obtained for the large grain sample

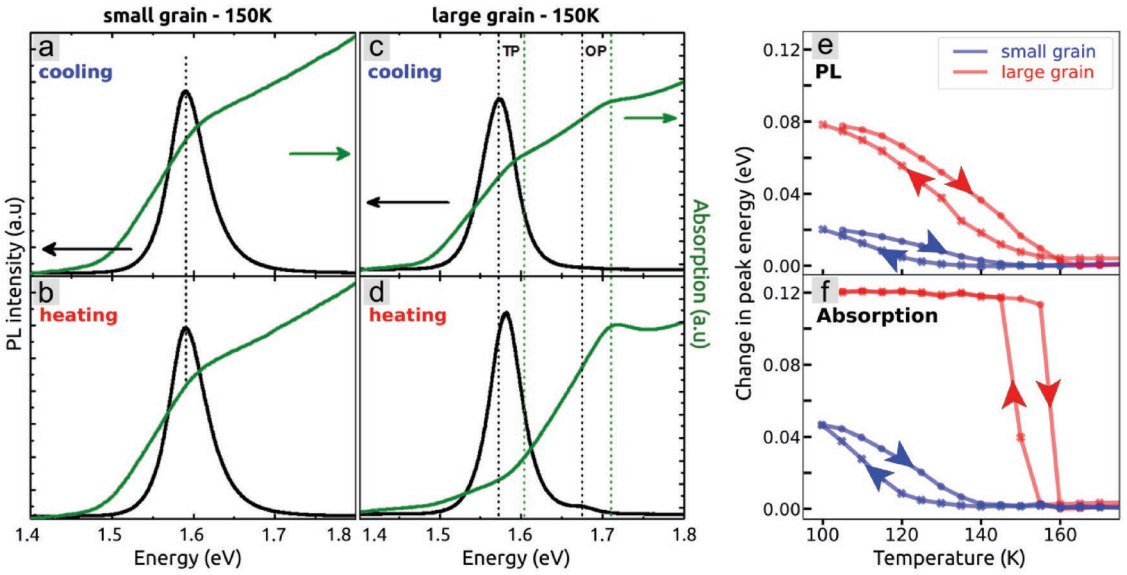

Figure 3. Comparison of absorption (green) and PL (black) spectra at 150 K while cooling and heating, respectively, for a,b) the small grain and c,d) large grain film. Dotted lines mark the central position of the PL peak(s) during the cooling phase as a reference point, and arrows indicate that the energy difference between the absorption onset and the PL energy is larger during the cooling phase than the heating up phase. e,f) Change in peak energy with temperature in PL and absorption, respectively. The energies were extracted from the spectra at each temperature, and the weighted average calculated in the presence of mixed peaks.

(bottom panel of Figure 2a) show a clear phase-transition hysteresis in absorption (shown by black dotted lines), coinciding with the apparition of an excitonic absorption peak around 1.7 eV (highlighted by a red dashed line). This phase transition is also observed in PL (bottom panel of Figure 2b) with the emergence of a second peak blue-shifted by about 50 meV with respect to the TP emission peak.[25] The coexistence of both phases is visible in PL from 130 K (when cooling down to 100 K) up to 145 K (when heating up to 300 K), which is overall in good agreement with XRD. We note a small shift in the temperature ranges between PL and XRD measurements, which we attribute to the fact that PL emphasizes any TP components, even small fractions, due to energy funneling of carriers from OP to TP.[31]

In **Figure 3** we show absorption (green) and PL (black) spectra at 150 K when cooling and heating, respectively, for both the small (a,b) and large grain (c,d) films. Dotted lines mark the central position of the PL peak and absorption onset during the cooling phase as a reference point for comparison. While there is no clear sign of phase transition hysteresis between the cooling and heating cycles in the small grain film at 150 K (Figure 3a,b), we observe clear differences in both PL and absorption in the large grain sample (Figure 3c,d). The emergence of the OP absorption edge upon cooling in the large grain sample shows that the phase transition has started at this temperature (Figure 3c); this is not seen in the PL because the presence of any TP component will dominate the emission. By contrast, at that same temperature but upon the heating cycle (Figure 3d), the TP absorption is diminished and the OP absorption peak dominates; the presence of a second PL peak (i.e., the OP emission) adds further evidence that the OP now constitutes a larger fraction of the film than it does at the same temperature during the cooling cycle.

In order to further characterize this phase transition behavior, we extract at each temperature the PL and absorption energy, and calculate the weighted average in the presence of any mixed OP and TP-related peaks. We summarize the results in Figure 3e,f and compare the overall change in energy from before to after the phase transition for the PL and absorption spectra, respectively (see Figure S9, Supporting Information). The amplitude of that change from both measurements is ≈5 times higher in the large grain (≈80–120 meV) than in the small grain sample (≈20 meV). We also note that the hysteresis in the small grain spreads again over a larger temperature range (≈75 K) when compared to the large (≈60 K) and medium (≈50 K) grain films, with an overall trend consistent with the observed structural changes (XRD). This widening of the hysteresis, and the decrease in the overall amplitude of the energy changes between the two phases, again suggests that the phase transition is more suppressed in the small grain sample.

In order to understand how the PL properties change with temperature at the microscale, we performed micro-PL measurements. We scanned the laser in steps of 2 μm and recorded at each location a PL spectrum in order to create 2D maps at a range of temperatures while cooling down from room temperature to 100 K and heating back up to room temperature. We performed a peak-detection and fitting routine on the data in each map in order to extract the statistically relevant peaks and relevant peak parameters (see Figures S2 and S10 and Table S3 of the Supporting Information for more details about the method). **Figure 4** shows the results obtained for the large grain film (see Figures S11 and S12 of the Supporting Information for medium and small grain samples, respectively), with the pure TP phase shown in blue. When both phases are present, the ratio of the OP peak area over the TP peak area is displayed with a linear color scale ranging from red (TP peak dominates)

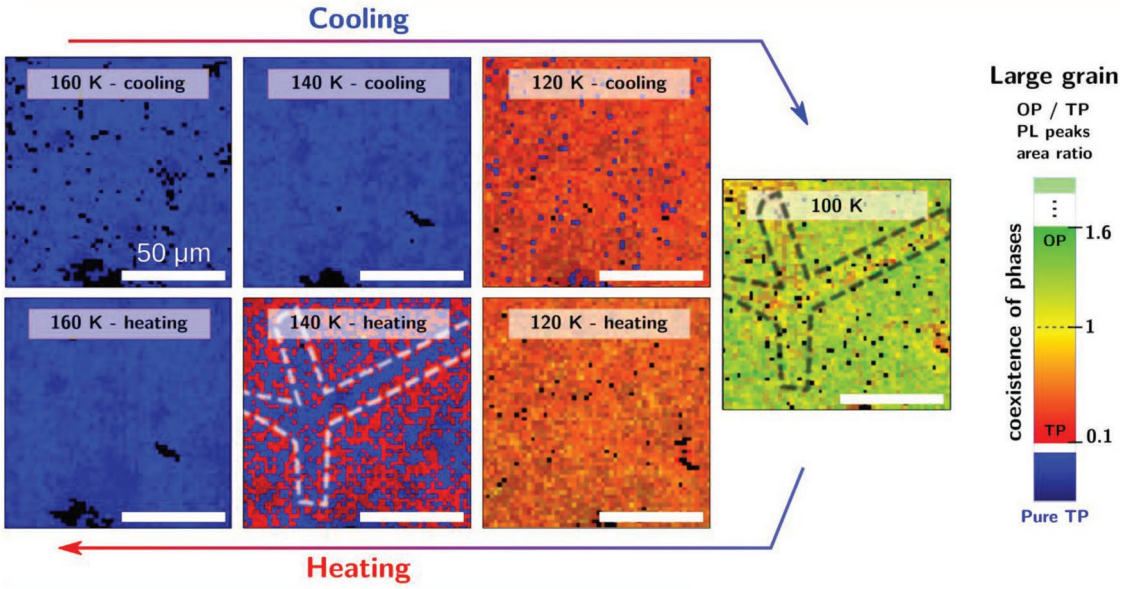

Figure 4. Temperature-dependent micro-PL measurements on the large grain film. A tightly focused 532 nm laser was used with an excitation density of 1500 mW cm^{-2}. We scanned the laser in steps of 2 µm and recorded at each location a PL spectrum in order to create 2D maps at 160, 140, 120, and 100 K while cooling down from room temperature to 100 K and heating back up to room temperature. Each spectrum was fitted with Gaussian functions, and the PL peak area(s) extracted. Regions of pure TP phase are in blue, and the ratio of the OP peak area over the TP peak area displayed with a linear color scale ranging from red to green when both phases coexist. The area circled by a dotted line highlights a region where the OP phase does not form very well even at 100 K and undergoes an early transition back to TP before 140 K (heating).

to green (OP peak dominates). When cooling down, the PL arises only from the TP phase until 120 K, at which point mixed phases become interspersed throughout, with a larger proportion of emission from TP across the film. An increased heterogeneity in the area ratio of the OP and TP peaks in the presence of mixed phases appear at 100 K where the OP emission peak dominates overall (with a OP/TP ratio ≈1.6), apart from some features such as the one highlighted by dotted lines where it remains smaller than the TP peak. Interestingly, this heterogeneity is less visible at 120 K (heating), but it stands out again at 140 K (heating), the temperature at which the hysteresis is also the most noticeable when comparing with the 140 K (cooling) map. The region highlighted by dashed lines where the OP peak was still smaller than the TP peak at 100 K is also the first to transition back to the pure TP phase at 140 K (heating). These micro-PL maps reveal the microscale complexities of this phase transition behavior and how sensitive the structure is to the local environment. Similar maps and analyses were performed on the medium (Figures S11 and S13, Supporting Information) and small grain films (Figures S12 and S14, Supporting Information). Again, no clear phase coexistence was seen on the small grain sample down to 100 K (Figure S14, Supporting Information).

Our collective results provide insight into how sensitively the optoelectronic and phase transition properties depend on the local environment of the material. We find that smaller grain $MAPbI_3$ samples show greater hysteretic effects, which are consistent with these small grains being constrained and inhibited from freely undergoing phase transitions; in contrast the phase transition is much more rapid and more easily performed in larger grain samples. This is consistent with our previous work, where we found that the hysteretic phase transition in a bulk $MAPbI_3$ film was reduced when the same film was scraped off into a powder form,[24] allowing the system to more freely transition. Furthermore, we performed similar temperature-dependent PL (Figure S15, Supporting Information) and X-ray diffraction (Figure S16, Supporting Information) measurements on mixed-cation $(FA_{0.80}MA_{0.15}Cs_{0.05})Pb(I_{0.83}Br_{0.17})_3$ samples (FA = formamidinium), which correspond to state-of-the-art solar cell devices. We find that these mixed cation films, which have grain sizes comparable to the medium grain samples (Figure S17, Supporting Information), also exhibit hysteresis around the low-temperature phase transition, though the magnitude of these effects are greatly reduced with respect to the $MAPbI_3$ medium-grain counterparts. These observations are consistent with the FA-based samples exhibiting a more rigid lattice than their MA-counterparts, thereby inhibiting the phase transition and associated hysteresis effects in a similar manner to the constrained small grain samples. Nevertheless, these results also demonstrate that such effects are still present and important even in the highest performing devices. The collective results strongly suggest that locally constraining the grains or rigidifying the lattice can inhibit the phase transition,[38] and in the extreme case of very small grains, can almost entirely suppress the phase transition. This reveals local strain as a lever for controlling phase behavior, which could be exploited in future optoelectronic device structures.[39,40] This work, focusing on low-temperature phase transitions, therefore provides unique insight into local strain properties, which ultimately lead to performance and stability issues at device operating temperatures. Our work also suggests that one must seek a compromise between constraining or rigidifying these soft systems to prevent the negative impact of phase transitions and defect formation (e.g., through smaller grains) while minimizing compressive strain and grain boundaries; the recent approaches to alloying perovskites systems through

mixed A-site cations and X-site halides may have serendipitously found this compromise, though further optimization is still required to eliminate the hysteresis effects entirely. Further work would also be required to elucidate the precise nature and magnitude of the strain involved in these phenomena.

We investigated the TP to OP phase transition in $MAPbI_3$ perovskite thin films with grain sizes ranging across two orders of magnitude from tens of nanometers to micrometer scale. By means of temperature-dependent X-ray diffraction, absorption, macro- and micro-photoluminescence measurements, we showed that the phase transition is increasingly suppressed with decreasing grain size. We also report that the hysteresis of both structural and optoelectronic properties widens across a larger temperature span with decreasing grain size. Micro-PL maps reveal a spatial heterogeneity in the presence of the mixed phase of the large grain film, providing a microscale visualization of the findings. Our work reveals the influence of the local environment on optoelectronic, physical, and phase properties of the perovskite structure, which is essential for phase and defect engineering in operating devices.

Supporting Information

Supporting Information is available from the Wiley Online Library or from the author.

Acknowledgements

C.S. and S.J.Z. contributed equally to this work. C.S. thanks the EPSRC (Nano-Doctoral Training Centre)a, and the Cambridge Trust. S.J.Z. acknowledges the support within the Etiuda 5 scholarship from the National Science Centre Poland (No. 2017/24/T/ST3/00257). S.D.S acknowledges the Royal Society and Tata Group (UF150033). The work was supported by a Royal Society International Exchanges Cost Share award (IEC\R2\170108). K.F. thanks the EPSRC, Cambridge Trust, the Winton Sustainability Program and the George and Lilian Schiff Foundation. This work was supported in part by BLAPHENE and STRABOT projects, which received funding from the IDEX Toulouse, Emergence program,\Programme des Investissements d'Avenir under the program ANR-11-IDEX-0002-02, reference ANR-10-LABX-0037-NEXT. The authors thank EPSRC for funding through grant EP/M05173/1. K.G. acknowledges support from the Polish Ministry of Science and Higher Education within the Mobilnosc Plus program (Grant No. 1603/MOB/V/2017/0). E.R. acknowledges the EPSRC for part funding. This project has received funding from the European Research Council (ERC) under the European Union's Horizon 2020 research and innovation programme (grant agreement number 756962).

Conflict of Interest

Samuel D. Stranks is a cofounder of Swift Solar, Inc.

Keywords

halide perovskites, optoelectronic properties, phase transition, photovoltaics, strain

Received: June 12, 2019
Published online: August 7, 2019

[1] L. K. Ono, N.-G. Park, K. Zhu, W. Huang, Y. Qi, *ACS Energy Lett.* **2017**, *2*, 1749.
[2] N. G. Park, M. Grätzel, T. Miyasaka, K. Zhu, K. Emery, *Nat. Energy* **2016**, *1*, 16152.
[3] S. D. Stranks, H. J. Snaith, *Nat. Nanotechnol.* **2015**, *10*, 391.
[4] Y. Zhao, J. Wei, H. Li, Y. Yan, W. Zhou, D. Yu, Q. Zhao, *Nat. Commun.* **2016**, *7*, 10228.
[5] P. Li, Y. Zhang, C. Liang, G. Xing, X. Liu, F. Li, X. Liu, X. Hu, G. Shao, Y. Song, *Adv. Mater.* **2018**, *30*, 1805323.
[6] P. Li, C. Liang, B. Bao, Y. Li, X. Hu, Y. Wang, Y. Zhang, F. Li, G. Shao, Y. Song, *Nano Energy* **2018**, *46*, 203.
[7] P. A. Mante, C. C. Stoumpos, M. G. Kanatzidis, A. Yartsev, *J. Phys. Chem. Lett.* **2018**, *9*, 3161.
[8] A. Létoublon, S. Paofai, B. Rufflé, P. Bourges, B. Hehlen, T. Michel, C. Ecolivet, O. Durand, S. Cordier, C. Katan, J. Even, *J. Phys. Chem. Lett.* **2016**, *7*, 3776.
[9] Y. Rakita, S. R. Cohen, N. K. Kedem, G. Hodes, D. Cahen, *MRS Commun.* **2015**, *5*, 623.
[10] M. Spina, A. Karimi, W. Andreoni, C. A. Pignedoli, B. Náfrádi, L. Forró, E. Horváth, *Appl. Phys. Lett.* **2017**, *110*, 121903.
[11] W. N. Sharpe, *2001 Proc. of Int. Semiconductor Device Research Symp. (ISDRS 2001)*, IEEE, Washington, DC **2001**.
[12] K. E. Petersen, *Micromechanics and MEMS: Classic and Seminal Papers to 1990*, Wiley/IEEE Press, New York **1997**.
[13] S. Sze, *Semiconductor Devices: Physics and Technology. Physics of Semiconductor Devices*, 2nd ed., Wiley, New York **2001**.
[14] T.-Y. Lai, Y.-J. Hsiao, T.-H. Fang, *Mater. Res. Express* **2017**, *4*, 115006.
[15] S. Luo, J.-H. Lee, C.-W. Liu, J.-M. Shieh, C.-H. Shen, T.-T. Wu, D. Jang, J. R. Greer, *Appl. Phys. Lett.* **2014**, *105*, 011907.
[16] I. V. Kurilo, V. P. Alekhin, I. O. Rudyi, S. I. Bulychev, L. I. Osypyshin, *Phys. Status Solidi Appl. Res.* **1997**, *163*, 47.
[17] A. M. Martínez, R. Soriano, R. Faccio, A. B. Trigubó, *Proc. Mater. Sci.* **2015**, *8*, 656.
[18] D. W. DeQuilettes, W. Zhang, V. M. Burlakov, D. J. Graham, T. Leijtens, A. Osherov, V. Bulović, H. J. Snaith, D. S. Ginger, S. D. Stranks, *Nat. Commun.* **2016**, *7*, 11683.
[19] E. T. Hoke, D. J. Slotcavage, E. R. Dohner, A. R. Bowring, H. I. Karunadasa, M. D. McGehee, *Chem. Sci.* **2015**, *6*, 613.
[20] C. Eames, J. M. Frost, P. R. F. Barnes, B. C. O'Regan, A. Walsh, M. Saiful Islam, *Nat. Commun.* **2015**, *4*, 7497.
[21] M. Anaya, J. F. Galisteo-López, M. E. Calvo, J. P. Espinós, H. Míguez, *J. Phys. Chem. Lett.* **2018**, *9*, 3891.
[22] X. Deng, X. Wen, C. F. J. Lau, T. Young, J. Yun, M. A. Green, S. Huang, A. W. Y. Ho-Baillie, *J. Mater. Chem. C* **2016**, *4*, 9060.
[23] P. Singh, N. M. Ravindra, *Sol. Energy Mater. Sol. Cells* **2012**, *101*, 36.
[24] A. Osherov, E. M. Hutter, K. Galkowski, R. Brenes, D. K. Maude, R. J. Nicholas, P. Plochocka, V. Bulović, T. J. Savenije, S. D. Stranks, *Adv. Mater.* **2016**, *28*, 10757.
[25] W. Kong, Z. Ye, Z. Qi, B. Zhang, M. Wang, A. Rahimi-Iman, H. Wu, *Phys. Chem. Chem. Phys.* **2015**, *17*, 16405.
[26] P. S. Whitfield, N. Herron, W. E. Guise, K. Page, Y. Q. Cheng, I. Milas, M. K. Crawford, *Sci. Rep.* **2016**, *6*, 35685.
[27] C. Qin, T. Matsushima, D. Klotz, T. Fujihara, C. Adachi, *Adv. Sci.* **2018**, *6*, 1801079.
[28] Y. Miyazawa, M. Ikegami, H. W. Chen, T. Ohshima, M. Imaizumi, K. Hirose, T. Miyasaka, *iScience* **2018**, *2*, 148.
[29] D. W. DeQuilettes, S. M. Vorpahl, S. D. Stranks, H. Nagaoka, G. E. Eperon, M. E. Ziffer, H. J. Snaith, D. S. Ginger, *Science* **2015**, *348*, 683.
[30] S. Y. Leblebici, L. Leppert, Y. Li, S. E. Reyes-Lillo, S. Wickenburg, E. Wong, J. Lee, M. Melli, D. Ziegler, D. K. Angell, D. F. Ogletree,

P. D. Ashby, F. M. Toma, J. B. Neaton, I. D. Sharp, A. Weber-Bargioni, *Nat. Energy* **2016**, *1*, 16093.
[31] K. Galkowski, A. A. Mitioglu, A. Surrente, Z. Yang, D. K. Maude, P. Kossacki, G. E. Eperon, J. T.-W. Wang, H. J. Snaith, P. Plochocka, R. J. Nicholas, *Nanoscale* **2017**, *9*, 3222.
[32] M. Vrucinic, C. Matthiesen, A. Sadhanala, G. Divitini, S. Cacovich, S. E. Dutton, C. Ducati, M. Atatüre, H. Snaith, R. H. Friend, H. Sirringhaus, F. Deschler, *Adv. Sci.* **2015**, *2*, 1500136.
[33] X. Ren, Z. Yang, D. Yang, X. Zhang, D. Cui, Y. Liu, Q. Wei, H. Fan, S. (Frank) Liu, *Nanoscale* **2016**, *8*, 3816.
[34] N. Giesbrecht, J. Schlipf, I. Grill, P. Rieder, V. Dyakonov, T. Bein, A. Hartschuh, P. Müller-Buschbaum, P. Docampo, *J. Mater. Chem. A* **2018**, *6*, 4822.
[35] K. Chen, S. Schünemann, S. Song, H. Tüysüz, *Chem. Soc. Rev.* **2018**, *47*, 7045.
[36] R. Brenes, D. Guo, A. Osherov, N. K. Noel, C. Eames, E. M. Hutter, S. K. Pathak, F. Niroui, R. H. Friend, M. Saiful Islam, H. J. Snaith, V. Bulovic, T. J. Savenije, S. D. Stranks, *Joule* **2017**, *1*, 155.
[37] E. Tennyson, T. Doherty, S. Stranks, *Nat. Rev. Mater.* **2019**, https://doi.org/s41578-019-0125-0.
[38] J. S. Bechtel, A. Van der Ven, *Phys. Rev. Mater.* **2018**, *2*, 025401.
[39] T. W. Jones, A. Osherov, M. Alsari, M. Sponseller, B. C. Duck, Y.-K. Jung, C. Settens, F. Niroui, R. Brenes, C. V. Stan, Y. Li, M. Abdi-Jalebi, N. Tamura, J. Emyr Macdonald, M. Burghammer, R. H. Friend, V. Bulović, A. Walsh, G. J. Wilson, S. Lilliu, S. D. Stranks, *Energy Environ. Sci.* **2019**, *12*, 596.
[40] B. Chen, T. Li, Q. Dong, E. Mosconi, J. Song, Z. Chen, Y. Deng, Y. Liu, S. Ducharme, A. Gruverman, F. De Angelis, J. Huang, *Nat. Mater.* **2018**, *17*, 1020.